Experimental Animals
Exp. Anim. 70(4), 498–507, 2021

Original

A diastolic dysfunction model in non-human primates with transverse aortic constriction

Nicole Tee Gui ZHEN[1)], Sze-Jie LOO[1)], Li-Ping SU[1)], Zhong-Hao TAO[2)], Fu GUI[3)], Jun-Hua LUO[4)] and Lei YE[1)]

[1)]*National Heart Research Institute Singapore, National Heart Centre Singapore, 5 Hospital Drive, 169609, Singapore*
[2)]*Department of Thoracic and Cardiovascular Surgery, Nanjing First Hospital, Nanjing Medical University, 68 Changle Road, 21006, Nanjing, Jiangsu, P.R. China*
[3)]*Department of Ophthalmology, The Second Affiliated Hospital of Nanchang University, No. 1 Minde Road, Donghu District, 330003, Nanchang, Jiangxi, P.R. China*
[4)]*Jiangxi Hospital of Integrated Traditional Chinese and Western Medicine, 90 Bayi Avenue, Xihu District, 330003, Nanchang, Jiangxi, P.R. China*

Abstract: Transverse aortic constriction (TAC) has been widely used to study cardiac hypertrophy, fibrosis, diastolic dysfunction, and heart failure in rodents. Few studies have been reported in preclinical animal models. The similar physiology and anatomy between non-human primates (NHPs) and humans make NHPs valuable models for disease modeling and testing of drugs and devices. In the current study, we aimed to establish a TAC model in NHPs and characterize the structural and functional profiles of the heart after TAC. A non-absorbable suture was placed around the aorta between the brachiocephalic artery and left common carotid artery to create TAC. NHPs were divided into 2 groups according to pressure gradient (PG): the Mild Group (PG=31.01 ± 12.40 mmHg, n=3) and the Moderate Group (PG=53.00 ± 9.37 mmHg, n=4). At 4 weeks after TAC, animals in both TAC groups developed cardiac hypertrophy: enlarged myocytes and increased wall thickness of the left ventricular (LV) anterior wall. Although both TAC groups had normal systolic function that was similar to a Sham Group, the Moderate Group showed diastolic dysfunction that was associated with more severe cardiac fibrosis, as evidenced by a reduced A wave velocity, large E wave velocity/A wave velocity ratio, and short isovolumic relaxation time corrected by heart rate. Furthermore, no LV arrhythmia was observed in either animal group after TAC. A diastolic dysfunction model with cardiac hypertrophy and fibrosis was successfully developed in NHPs.
Key words: diastolic dysfunction, fibrosis, hypertrophy, transverse aortic constriction

Introduction

The prevalence of heart failure (HF) is rising and will continue to do so with the growing global trend toward aging populations. According to NHANES data, approximately 6.2 million American adults experienced HF between 2013 and 2016 compared with 5.7 million between 2009 and 2012 [1]. Currently, HF is classified into three phenotypes based on the measured value for the left ventricle (LV) ejection fraction (EF): heart failure with reduced ejection fraction (HFrEF), LVEF <40%; heart failure with mid-range ejection fraction, LVEF 40–49%; and heart failure with preserved ejection fraction (HFpEF), LVEF ≥50% [2]. Left ventricular diastolic dysfunction (LVDD) is recognized as one of the important mechanisms responsible for symptoms in patients with HFpEF. It is caused by impaired LV relaxation, which results in increased LV stiffness with reduced cardiac output and/or elevated intracardiac pressures at rest or during stress [3]. Its phenotype is associated with increased interstitial fibrosis with deposition of collagen and modified extracellular matrix

(Received 15 March 2021 / Accepted 17 May 2021 / Published online in J-STAGE 15 June 2021)
Corresponding author: L. Ye. e-mail: yeleislp@yahoo.com

proteins that frequently, but not necessarily always, result in LV concentric remodeling/hypertrophy and atrial enlargement [4].

Numerous animal studies have used a transverse aortic constriction (TAC) model to study cardiac hypertrophy, fibrosis, diastolic dysfunction, and HFpEF [5–7]. Most of these studies were performed on rodents, as they are widely available transgenic models with short life cycles and larger sample sizes [8, 9]. However, a very important drawback of a rodent model is the anatomical and physiological differences between them and humans, including faster heart rates, different metabolism, and small size of the organs in rodents, which make direct translation of interventional and surgical procedures into clinical practice impossible at times. Therefore, extrapolating data and replicating results from small animal models to large mammals and humans are often difficult.

Thus, large animal models, such as the non-human primates (NHPs), are essential for translational cardiovascular research, as their anatomy, physiology, function, and metabolism more closely resemble those of humans [10, 11]. They have been studied for decades as models to understand the pathogenesis and progression of cardiovascular diseases [10, 12] and kidney disability [13]. Therefore, in the current study, we developed TAC models in NHPs and characterized cardiac functional and structural changes.

Materials and Methods

Creating a monkey heart model of TAC

The animal experimental protocol was approved by the Institutional Animal Care and Use Committee of the Singapore Health Services Pte Ltd., Singapore. All animal experimental procedures were performed in accordance with the ARRIVE guidelines and conformed to the guidelines from Directive 2010/63/EU of the European Parliament on the protection of animals used for scientific purposes or the current NIH guidelines.

Experimental TAC was induced in 9 adult NHP (*Macaca fascicularis*). The monkeys were sedated with a mixture of ketamine (10 mg/kg)/medetomidine (0.1 mg/kg). After intubation, anesthesia was maintained using 2–2.5% isoflurane. After disinfecting the chest, an incision was performed between ribs 2 and 3 to expose the aortic arch. A non-absorbable suture was placed around the aorta between the brachiocephalic artery and left common carotid artery. A 23G or 25G blunt needle was placed between the suture and aortic arch and was removed after the suture was tied to create TAC (Fig. 1A). Then, the chest was closed in layers using absorbable sutures. Surviving NHPs were divided into 2 groups according to pressure gradient (PG): Mild Group (15 mmHg < PG < 40 mmHg, n=3) and Moderate Group (40 mmHg < PG < 70 mmHg, n=4). Two monkeys died immediately after TAC surgery due to acute heart failure. Monkeys that were matched for age and body weight (n=3) and only underwent open-chest surgery served as the Sham Group (control).

Real-time electrocardiogram monitoring

Implantable loop recorders (Reveal, Medtronic, Minneapolis, MN, USA) were subcutaneously placed in the left paraspinal area inferior to the angle of the scapula in the NHPs after surgery. The recorded electrocardiogram data from the loop recorders were transmitted to a server once every two days. The incidences of ventricular arrhythmia were analyzed.

Left ventricular function assessment by echocardiography

All monkeys were sedated by mixture of ketamine (10 mg/kg)/medetomidine (0.1 mg/kg), and anesthesia was maintained using 2–2.5% isoflurane. Transthoracic echocardiography was performed at baseline (before surgery) and 4 weeks after surgery on all monkeys using a Vivid E93 echocardiographic system and a 6S-D phased array transducer with a frequency spectrum of 2.4–8.0 MHz (GE Venged Ultrasound AS, Horten, Norway). The monkeys were placed in the supine position with their chest shaved and a layer of acoustic coupling gel applied to the thorax. An average of 10 cardiac cycles of 2 dimensional images at all standard echocardiographic views (parasternal long and short axis, 4, 2 and 3 chambers) were acquired and stored for subsequent offline analysis. Two-dimensional guided m-mode of the parasternal short axis at the mid-papillary muscle level was used to obtain measurements, including the interventricular septal thickness, LV internal diameters during diastole (LVIDd) and systole (LVIDs), and left ventricular posterior wall thicknesses at systole and diastole. Based on these measurements, the left ventricular EF, fractional shortening (FS), and left ventricular mass were obtained and calculated by the American Society of Echocardiography-corrected cube formula [14].

Mitral inflow and aortic outflow profiles were acquired using pulsed Doppler in the apical four-chamber view, with the sample volume placed at the mitral tip level at baseline (before surgery) and 4 weeks after surgery. The LV index was calculated as the LV mass normalized to body weight. Transmitral flow of the early (E) and late (A) diastolic filling velocities and the E/A ratio were measured as previously described [15]. Isovolumic relaxation time (IVRT), isovolumic contraction time

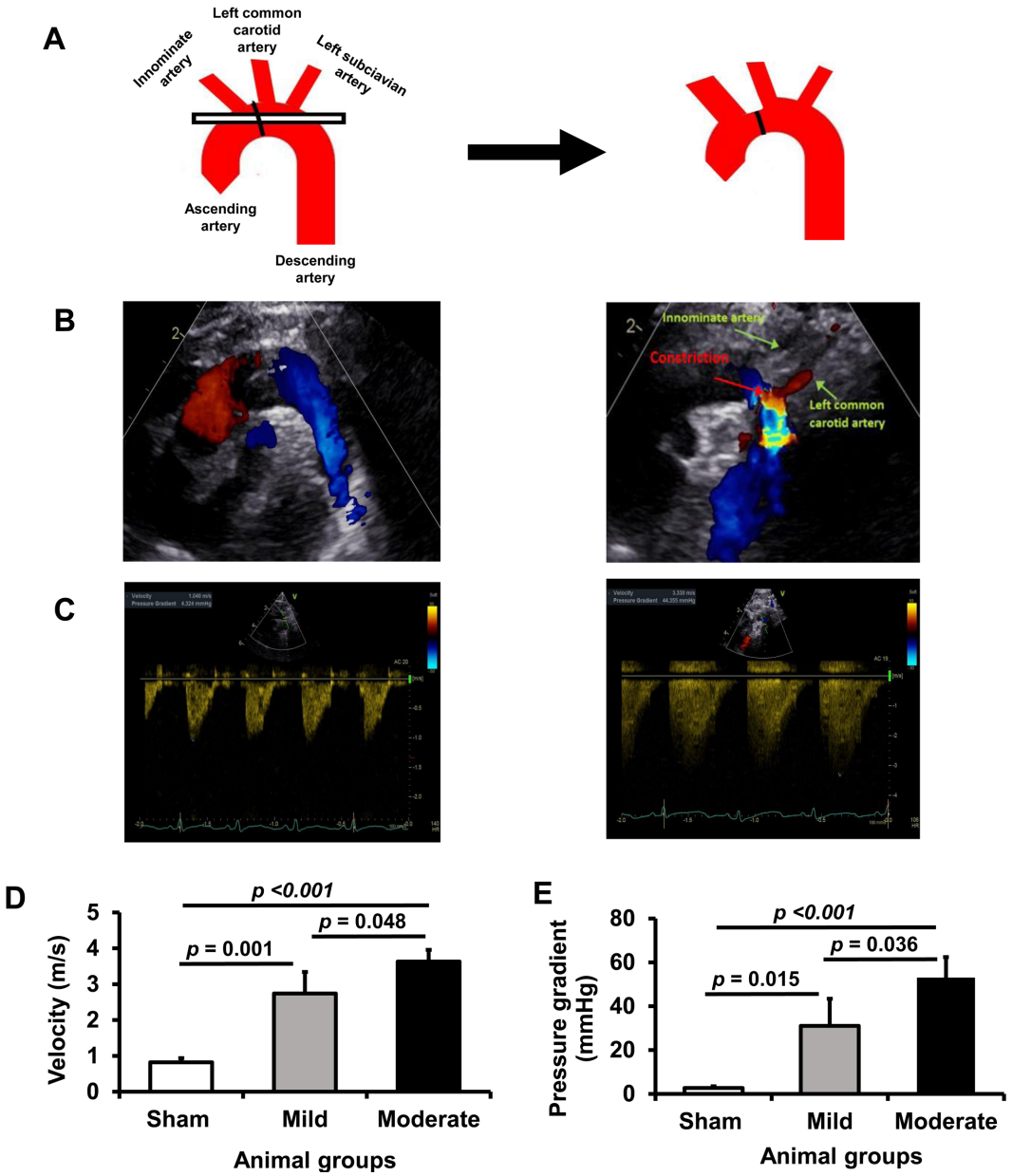

Fig. 1. Establishing a monkey heart model of transaortic constriction (TAC). (A) A schematic presentation of TAC surgery on the monkey aortic arch. (B) Representative 2D color Doppler for visualization of the TAC site. (C) Representative continuous-wave Doppler for measurement of the peak velocity distal to the constriction, which was used to calculate pressure gradient. (D) Peak velocity distal to the constriction. (E) Pressure gradient was calculated using the modified Bernoulli equation (PG=4*Velocity^2) after TAC or sham surgery. Data are presented as the mean ± SD, and they were analyzed by one-way ANOVA among the 3 groups.

(IVCT), and aortic ejection time were also measured, and IVRT was corrected (IVRTc) for heart rate according to the formula (IVRTc=IVRT/√RR%). Subsequently, the transducer was placed at the suprasternal notch to visualize the transverse aortic arch. Guided by color flow Doppler, the peak velocity (V) distal to the constriction was measured with continuous wave Doppler to calculate the peak pressure gradient using the modified Bernoulli equation: $\Delta P=4 \times V^2$ [16]. All measurements were averaged for 3 cardiac cycles by a blinded operator.

Tissues

After the final echo study, the monkeys' hearts were arrested under anesthesia (2–2.5% isoflurane) by injecting 100 mg/ml/kg potassium chloride, explanted, and weighed. Cardiac tissue was either embedded into paraffin for immunohistochemistry studies or subjected to RNA or protein extraction for quantitative reverse transcription polymerase chain reaction (qRT-PCR) and collagen quantification.

Cardiac fibrosis assessment

Histochemical assessment: A Sirius Red/Fast Green Collagen (Chondrex, Woodinville, WA, USA) staining kit was used to visualize fibrotic tissue in the monkey LV. Paraffin sections with a thickness of 7 μm were dewaxed and stained as per the supplier's instruction [16–18].

qRT-PCR: RNA isolation and cDNA synthesis were performed as described previously [19], and PCR thermal cycling was conducted with the following primers: GACGGATTCCAGTTCGAGTATG, forward, and TTCTTGCAGTGGTAGGTGATG, reverse, for collagen type I alpha 1 (*COL1A1*) and GCTCTGCTTCATCCCACTATTA, forward, and CTGGCTTCCAGACATCTCTATC, reverse, for collagen type III alpha 1 (*COL3A1*).

Thermal cycling was performed 40 times, and each cycle consisted of enzyme activation at 95°C for 15 min, denaturation at 95°C for 30 s, annealing at 60°C for 30 s and extension at 72°C for 30 s. Endogenous *GAPDH* (GGGTGTGAACCATGAGAAGTAT, forward, and GAGTCCTTCCACGATACCAAAG, reverse) levels were used as an internal control for normalization [19]. *COL1A1* and *COL3A1* gene expression levels were normalized to *GAPDH* and presented as fold change relative to the Sham Group, the levels of which was set as 1.

Quantification of total collagen: Collagen from the LV anterior wall tissue was quantified using a Total Collagen Assay kit (QuickZyme Biosciences, Leiden, Netherlands) as described previously [16]. Briefly, the tissues were loaded into 6 M HCl and incubated for 20 h at 95°C in a thermo-block. Tissues were then vortexed and the total lysates were centrifuged for 10 min at 13,000 g to collect the supernatants for analysis as per the instructions.

Assessment of monkey cardiomyocyte hypertrophy

To determine myocyte hypertrophy, paraffin sections were stained with mouse IgM anti-α-sarcomere actin (α-SA). Images of monkey cardiac tissue were taken at anterior and posterior walls for analyzing cardiomyocytes (CM) size using an Olympus microscope (Olympus, Sapporo, Japan). CM diameter and nucleus area were measured using the ImageJ software [20]. Measurements were made for the anterior and posterior wall sections of the left ventricle.

Statistical analysis

Data were calculated and expressed as the mean ± SD. Comparisons among groups were analyzed for significance by one-way analysis of variance (ANOVA) with Tukey correction. The statistical analyses were performed with the IBM SPSS statistical software (version 20). A $P<0.05$ was considered significant.

Results

Profile of heart function change

All animals were found to have similar body weights, heart rates (HRs), and LV masses at baseline (Table 1).

Systolic function: Doppler echocardiography was performed to confirm the effectiveness of aortic constriction (Fig. 1b). After TAC, the blood flow velocity was

Table 1. Left ventricular systolic function

	Sham PG ≤ 5 mmHg n=3		Mild 15 mmHg ≤ PG ≤ 40 mmHg n=3		Moderate PG ≥ 40 mmHg n=4	
	Baseline	4 Weeks	Baseline	4 Weeks	Baseline	4 Weeks
Sex	F=1 and M=2		F=1 and M=2		F=2 and M=2	
Body weight (kg)	2.46 ± 0.48	2.62 ± 0.74	2.85 ± 0.28	2.67 ± 0.4	2.35 ± 0.05	2.38 ± 0.22
Antd (cm)	0.4 ± 0.08	0.38 ± 0.04	0.43 ± 0.08	0.57 ± 0.09*	0.42 ± 0.09	0.65 ± 0.06**
Ants (cm)	0.56 ± 0.11	0.58 ± 0.17	0.54 ± 0.09	0.74 ± 0.18	0.58 ± 0.08	0.83 ± 0.14
PLVWd (cm)	0.41 ± 0.06	0.4 ± 0.06	0.46 ± 0.1	0.49 ± 0.12	0.4 ± 0.09	0.47 ± 0.07
PLVWs (cm)	0.48 ± 0.06	0.5 ± 0.1	0.57 ± 0.06	0.71 ± 0.09	0.57 ± 0.12	0.63 ± 0.08
LVIDd (cm)	1.42 ± 0.36	1.55 ± 0.27	1.38 ± 0.1	1.35 ± 0.26	1.39 ± 0.11	1.23 ± 0.11
LVIDs (cm)	0.88 ± 0.36	0.97 ± 0.32	0.91 ± 0.13	0.77 ± 0.31	0.81 ± 0.14	0.69 ± 0.09
LV mass (g)	7.8 ± 2.35	8.07 ± 1.68	8.23 ± 1.6	10.05 ± 2.7	7.61 ± 2.09	10 ± 2.74
LV index (g/kg)	3.14 ± 0.54	3.13 ± 0.41	2.89 ± 0.48	3.38 ± 0.26	3.22 ± 0.83	4.17 ± 0.91
EF (%)	62.72 ± 10.67	60.46 ± 14.98	56.36 ± 9.1	68.07 ± 14.31	64.4 ± 11.37	67.84 ± 8.26
FS (%)	39.45 ± 8.55	38.03 ± 12.85	34.2 ± 7.15	44.44 ± 12.17	41.07 ± 0.27	43.73 ± 7.38
Hear rate (/min)	145.67 ± 3.05	128.33 ± 19.35	114.67 ± 16.8	108.33 ± 17.39	138.25 ± 15.84	112.75 ± 17.5

F, Female; M, Male; Antd, anterior wall thickness at end diastole; Ants, anterior wall thickness at end systole; PLVWd, posterior wall thickness at end diastole; PLVWs, posterior wall thickness at end systole; LVIDd, left ventricle internal diameter at end diastole; LVIDs, left ventricle internal diameter at end systole; LV, left ventricle; EF, ejection fraction; FS, fractional shortening; HR, heart rate. Data are presented as the mean ± SD. *$P<0.05$ and **$P\leq0.01$ as compared with the Sham group at 4 weeks after surgery using one-way ANOVA.

significantly increased in the Mild and Moderate Groups, increasing to 2.74 ± 0.6 m/s and 3.63 ± 0.33 m/s, respectively, as compared with the Sham Group (0.82 ± 0.12 m/s) (Figs. 1C and D). The corresponding PGs were 31.01 ± 12.40 mmHg and 53.00 ± 9.37 mmHg in the Mild and Moderate Groups, respectively (Fig. 1E). Notably, the velocity and PG of the Moderate Group were significantly high as compared with the Mild Group.

The increased PGs were associated with LV anterior and posterior wall thickening. Notably, the LV anterior wall thickness was significantly increased in both TAC groups as compared with the Sham Group at 4 weeks after surgery (Table 1). The LV internal diameter showed a trend toward decreasing in the TAC groups as compared with the Sham Group at 4 weeks after surgery. This was accompanied by an insignificant increase in LV mass or LV index in both animal groups after TAC surgery. These results indicate that concentric hypertrophy was developed in the Mild and Moderate Groups at 4 weeks post-TAC. Although cardiac hypertrophy was observed in both the Mild and Moderate Groups, LVEF and FS were still within normal ranges and were similar to those of the Sham Group at baseline and 4 weeks after surgery, indicating that animals in both TAC groups were in the compensated hypertrophy stage.

Diastolic function: Based on analysis of mitral inflow images (Fig. 2A), animals in the Mild Group showed a significantly small early mitral inflow peak velocity (E wave) and similar A wave velocity and E/A ratio as compared with the Sham Group at 4 weeks after TAC (Figs. 2B and C). Animals in the Moderate Group showed a significantly larger E wave velocity than the Mild Group (Fig. 2B). Although no significant change was observed in A wave velocity or E/A ratio in the Moderate Group, both showed trends toward decreasing or increasing as compared with the Sham or Mild Group at 4 weeks after

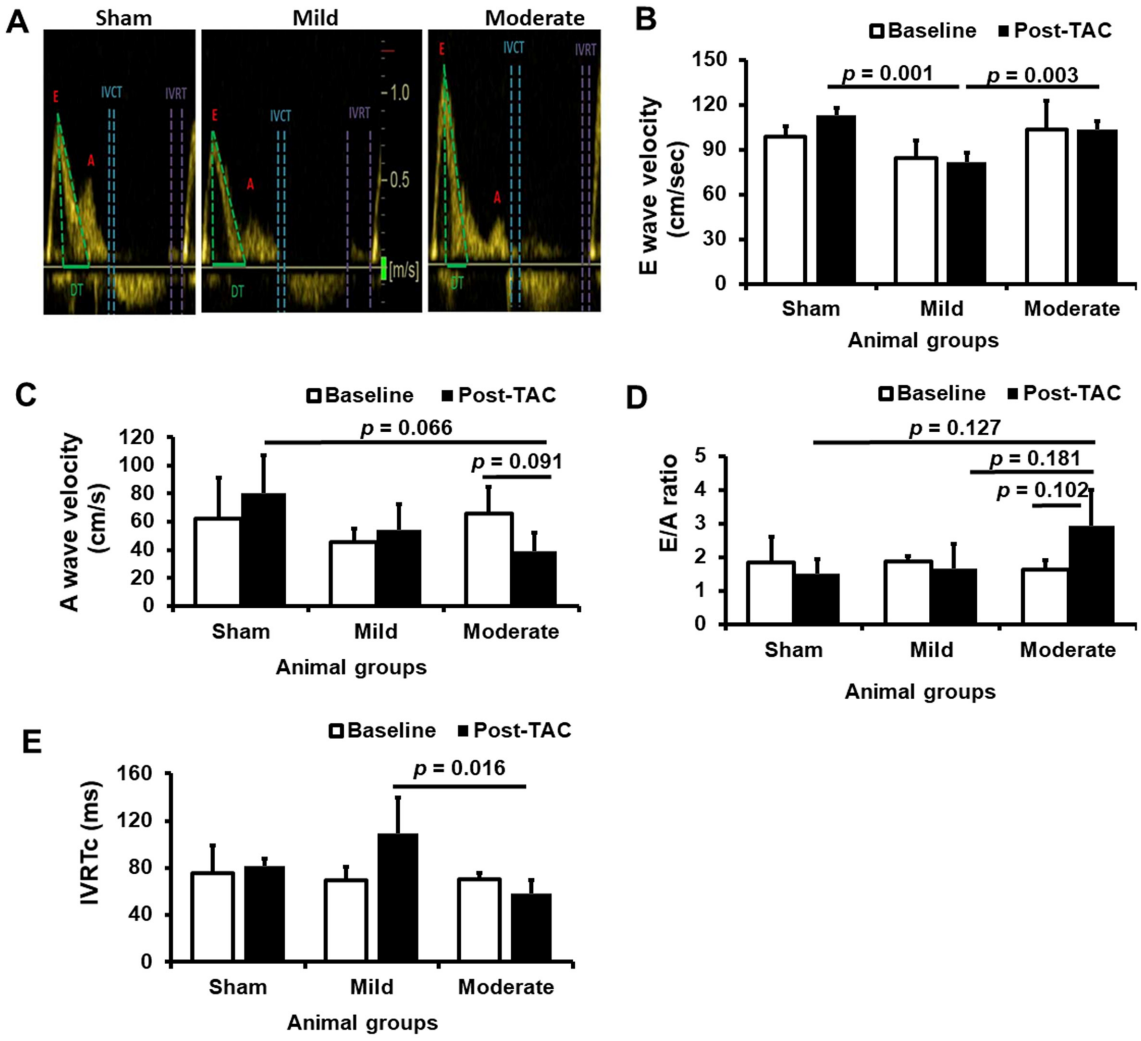

Fig. 2. Diastolic function of the three animal groups. (A) Representative images of mitral inflow patterns in the Sham, Mild, and Moderate Groups. (B) E wave velocity. (C) A wave velocity. (D) E/A ratio. (E) Isovolumic relaxation time corrected by heart rate (IVRTc). Data are presented as the mean ± SD, and they were analyzed by one-way ANOVA among the 3 groups. The paired t-test was performed for comparisons within the same group.

surgery or compared with themselves at baseline (Figs. 2C and D). A significantly reduced IVRTc was observed in the Moderate Group at 4 weeks after TAC as compared with the Mild Group, which had a prolonged IVRTc (Fig. 2E). These results suggested that the Moderate Group had more severe diastolic dysfunction as compared with the Mild Group at 4 weeks after TAC.

Cardiac hypertrophy after TAC surgery

M-mode echocardiogram showed that LV wall thickness, especially the anterior wall thickness, was significantly increased in both the Mild and Moderate Groups at 4 weeks after TAC (Figs. 3A and B; Table 1). Myocyte staining revealed that both TAC groups showed trends toward an increased myocyte size and myocyte nucleus

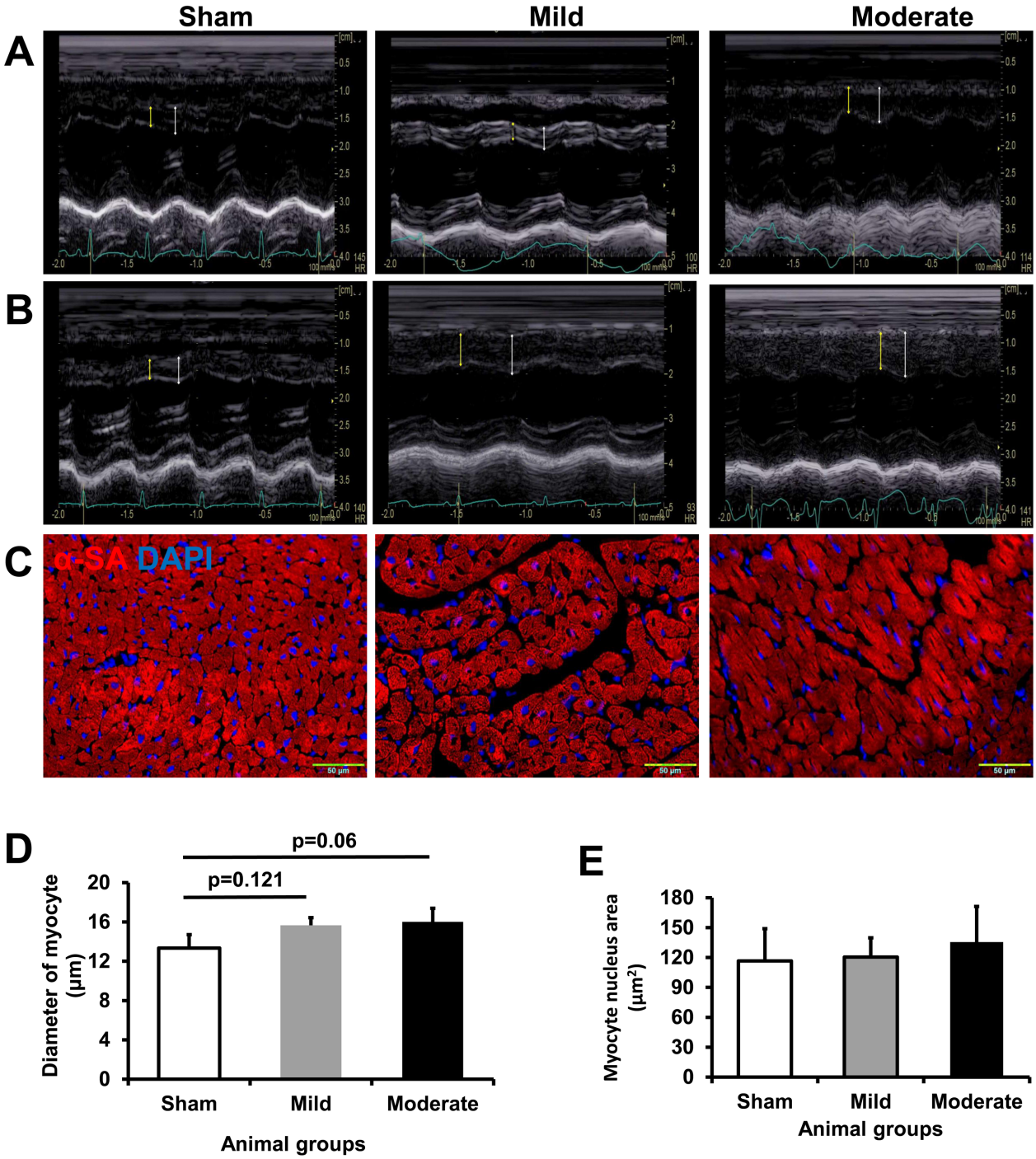

Fig. 3. Myocardial hypertrophy in the monkey heart after TAC. M-mode echocardiogram showing the left ventricular anterior wall thickness at baseline (A) and 4 weeks (B) after TAC or sham surgery. (C) Representative images of myocytes stained positive for α-sarcomere actin (α-SA). (D) Quantification of myocyte diameter. (E) Quantification of myocyte nucleus area. Bar=50 μm. Yellow line, anterior wall thickness at diastole; white line, anterior wall thickness at systole. Data are presented as the mean ± SD, and they were analyzed by one-way ANOVA among the 3 groups.

area as compared with the Sham Group at 4 weeks after TAC (Figs. 3C–E). However, no significant difference was observed among any of the groups.

Increased cardiac fibrosis in NHPs after TAC

Masson's trichrome and Sirius Red/Fast Green Collagen stainings showed increased myocardial fibrosis in both the Mild and Moderate Groups (Figs. 4A–D). qRT-PCR showed that although gene expression levels of collagen types 1 and 3 were upregulated in both TAC groups, significance was only observed in the Moderate Group as compared with the Sham Group (Fig. 4E). Consistently, quantification of collagen showed that the Moderate Group had a significantly increased collagen content in the LV anterior myocardium than the other two groups (Fig. 4F).

TAC did not induce ventricular arrhythmia

All the animals in the Sham Group had normal heart rhythms up to 4 weeks of observation. One animal in the Mild Group had bigeminal premature ventricular contractions (PVC; n=8) and isolated PVCs (n=17), while only one PVC was observed in the Moderate Group during the 4 weeks after TAC surgery (Figs. 5A–C). Thus, it seems that TAC-induced cardiac hypertrophy did not induce ventricular arrhythmia in NHPs during the compensated hypertrophy stage.

Discussion

In the present study, we showed that NHPs developed cardiac hypertrophy, fibrosis, and diastolic dysfunction with normal systolic function at 4 weeks after TAC, especially NHPs in the Moderate Group (40 mmHg < PG < 70 mmHg). These results indicate that a diastolic dysfunction model was successfully developed in NHPs.

Although the rodent TAC heart model has been extensively used to study cardiac hypertrophy, few studies have been carried out in large animal models. The current study is the first to report the establishment of TAC in NHPs. NHPs more closely resemble humans in terms of anatomy, physiology, cognitive function, and metabolism as compared with rodents [10]. The establishment of NHP TAC models enables more comprehensive characterization of structural and functional phenotypes associated with hypertrophy or diastolic dysfunction using advance imaging systems, such as positron emission tomography/computed tomography or magnetic resonance imaging.

We induced TAC in NHPs and characterized their cardiac functional and structural profiles. We divided the animals into 2 groups according to PG after TAC and found that although both groups had normal systolic function and developed cardiac hypertrophy, more severe fibrosis and diastolic dysfunction were observed in the Moderate Group at 4 weeks after TAC.

Left ventricular mass and index increased by 24.5% and 8% in the Mild Group and 23.9% and 33.2% in the Moderate Group as compared with the Sham Group at 4 weeks after TAC. This was the result of LV wall thickening, especially thickening of the LV anterior wall, which increased by 50% and 71.5% in the Mild and Moderate Groups, respectively. These results were supported by cellular changes, as myocytes at the LV anterior wall grew in size by 17.6% and 19.9% in the Mild and Moderate Groups, respectively, as compared with the Sham Group. This demonstrates that the PGs in both the Mild and Moderate Groups induced a similar level of cardiac hypertrophy.

Cardiac fibrosis is a typical phenotype seen in animal heart models of TAC [16]. Consistent with this, we found that collagen gene and protein expression levels were upregulated in TAC animals, especially in the Moderate Group, as a higher PG is associated with severe cardiac fibrosis [9]. Increased cardiac fibrosis causes myocardial stiffness, which results in systolic and diastolic dysfunction [9, 21].

Surprisingly, the systolic functions of both TAC groups were still within the normal ranges at 4 weeks after TAC. This appears to indicate that a mean PG of 53 mmHg is well tolerated by NHPs within 4 weeks after TAC. Although NHPS developed concentric hypertrophy, their systolic heart functions are still normal. However, we observed diastolic dysfunction, especially in the animals in the Moderate Group. As mitral inflow reflects the pressure difference between the atria and the ventricle, we measured the changes in the velocity and shape of the mitral Doppler inflow signal to determine the presence of diastolic dysfunction and its severity. We did not use the deceleration time (DT) of the E wave normalized for cycle length, as ideally DT is used when the heart rate is between 100–120 bpm [22, 23]; most of the monkeys had heart rates>120 bpm in the current study.

It was found that in the Mild group, TAC-induced pressure overload in the LV decreased the amount of blood moving from the LA to the LV during the early filling phase (E wave), with the majority of filling occurring during the atrial contraction phase (A wave). This manifests as a reduced mitral E wave velocity with a tall A wave velocity. It also took longer for the atrial pressure to reach to the level to initiate filling, which in turn prolonged IVRTc. On the other hand, exacerbated by increased cardiac fibrosis, the Moderate Group experienced even far greater pressure overload, which re-

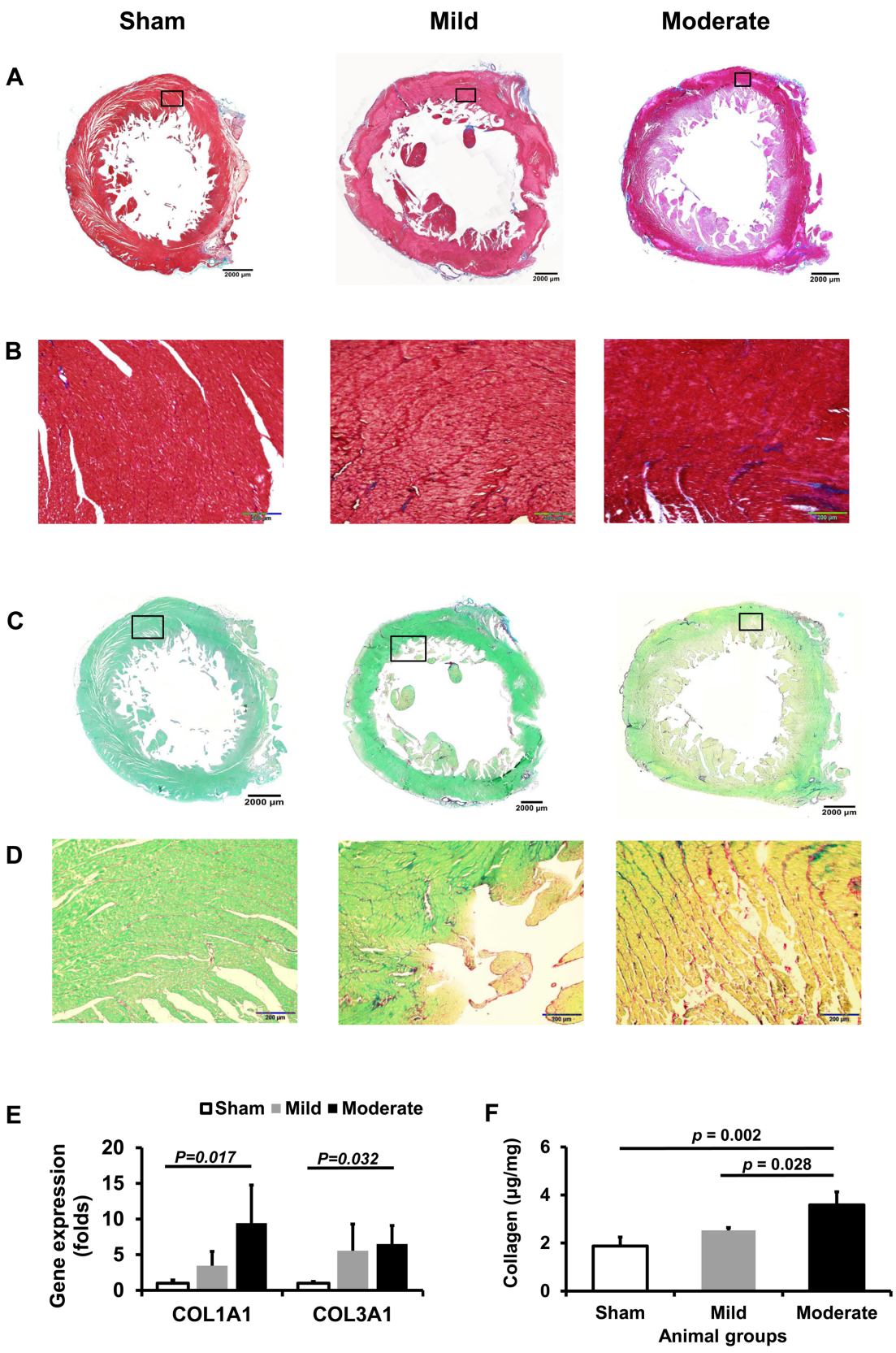

Fig. 4. Fibrosis in the monkey hearts. (A) Masson's trichrome staining of monkey heart tissues. (B) Magnified images of selected areas of Masson's trichrome staining. (C) Sirius Red/Fast Green Collagen staining of monkey heart tissues. (D). Magnified images of selected areas of Sirius Red/Fast Green Collagen staining. (E) Gene expression levels of alpha-1 type I collagen (*COL1A1*) and alpha-1 type 3 collagen (*COL3A1*) in the anterior wall of monkey myocardium at 4 weeks after surgery. (F) Total collagen content in the anterior wall of monkey myocardium at 4 weeks after surgery. Bars=2,000 μm in A and C and bars = 200 μm in B and C. Data are presented as the mean ± SD, and they were analyzed by one-way ANOVA among the 3 groups.

Fig. 5. Representative ECG images from loop recorders. (A) Normal monkey heart rate and rhythm. (B) Premature ventricular contractions. (C) Bigeminal premature ventricular contractions.

sulted in a tall E-wave and short A-wave. As the filling pressures were high, flow into the ventricle started early, and filling terminated quickly, which led to a shortened IVRTc. These results indicate severe diastolic dysfunction, grade IV, developed in the Moderate Group due to a higher LV filling pressure [22–24].

An examination of heart function revealed that left ventricular diastolic dysfunction with an EF≥50% in animals in the Moderate group, suggesting that an HFpEF-like phenotype was developed [2]. The normal EF levels suggested that the animals were in the compensated hypertrophy stage in the Moderate group and that the diastolic function was due to cardiac hypertrophy and fibrosis. Eventually, HFrEF may have developed in the Moderate Group in the decompensated hypertrophy stage. Although LVDD has been recognized to be an important symptom in patients with HFpEF, the mechanism is poorly understood due to limited access to human myocardial biopsies and the lack of animal models that fully mimic the human pathology. Patients with HFpEF are often asymptomatic, making early diagnosis difficult and therefore longitudinal follow-up studies nearly impossible [4]. Detection is usually based on clinical symptoms, such as fatigue and dyspnea, that may be accompanied by elevated jugular pressure, pulmonary crackles, and peripheral edema, which often occurr during the advanced stage of the disease [4]. Thus, this monkey heart model of TAC has potential to be a large animal model of HFpEF for screening and testing of drugs.

This study has a few limitations. The first is the small number of animals studied in each group. The second limitation of this study is that it is unknown whether NHPs with TAC would progress from compensated hypertrophy to decompensated hypertrophy.

Conclusions

We developed a TAC model in NHPs and showed that the animals developed diastolic dysfunction, cardiac hypertrophy, and fibrosis at 4 weeks after TAC, especially those with a moderate PG.

Funding

This study was funded by the Charles Toh Cardiovascular Fellowship Fund.

Disclosure of Interest

None.

Acknowledgments

The study was supported by Disease Model Core, National Heart Research Institute Singapore.

References

1. Benjamin EJ, Muntner P, Alonso A, Bittencourt MS, Callaway CW, Carson AP, et al. American Heart Association Council on Epidemiology and Prevention Statistics Committee and Stroke Statistics Subcommittee. Heart Disease and Stroke Statistics-2019 Update: A Report From the American Heart Association. Circulation. 2019; 139: e56–e528. [Medline] [CrossRef]
2. Ponikowski P, Voors AA, Anker SD, Bueno H, Cleland JGF, Coats AJS, et al. ESC Scientific Document Group. 2016 ESC Guidelines for the diagnosis and treatment of acute and chronic heart failure: The Task Force for the diagnosis and treatment of acute and chronic heart failure of the European Society of Cardiology (ESC)Developed with the special contribution of the Heart Failure Association (HFA) of the ESC. Eur Heart J. 2016; 37: 2129–2200. [Medline] [CrossRef]
3. Jeong EM, Dudley SC Jr. Diastolic dysfunction. Circ J. 2015;

79: 470–477. [Medline] [CrossRef]
4. Butler J, Fonarow GC, Zile MR, Lam CS, Roessig L, Schelbert EB, et al. Developing therapies for heart failure with preserved ejection fraction: current state and future directions. JACC Heart Fail. 2014; 2: 97–112. [Medline] [CrossRef]
5. Bao D, Lu D, Liu N, Dong W, Lu YD, Qin C, et al. Tomoregulin-1 prevents cardiac hypertrophy after pressure overload in mice by inhibiting TAK1-JNK pathways. Dis Model Mech. 2015; 8: 795–804. [Medline]
6. You J, Wu J, Zhang Q, Ye Y, Wang S, Huang J, et al. Differential cardiac hypertrophy and signaling pathways in pressure versus volume overload. Am J Physiol Heart Circ Physiol. 2018; 314: H552–H562. [Medline]
7. Rockman HA, Wachhorst SP, Mao L, Ross J Jr. ANG II receptor blockade prevents ventricular hypertrophy and ANF gene expression with pressure overload in mice. Am J Physiol. 1994; 266: H2468–H2475. [Medline]
8. Schiattarella GG, Altamirano F, Tong D, French KM, Villalobos E, Kim SY, et al. Nitrosative stress drives heart failure with preserved ejection fraction. Nature. 2019; 568: 351–356. [Medline] [CrossRef]
9. Richards DA, Aronovitz MJ, Calamaras TD, Tam K, Martin GL, Liu P, et al. Distinct Phenotypes Induced by Three Degrees of Transverse Aortic Constriction in Mice. Sci Rep. 2019; 9: 5844. [Medline] [CrossRef]
10. Cox LA, Olivier M, Spradling-Reeves K, Karere GM, Comuzzie AG, VandeBerg JL. Nonhuman Primates and Translational Research-Cardiovascular Disease. ILAR J. 2017; 58: 235–250. [Medline] [CrossRef]
11. Nakayama S, Koie H, Kato-Tateishi M, Pai C, Ito-Fujishiro Y, Kanayama K, et al. Establishment of a new formula for QT interval correction using a large colony of cynomolgus monkeys. Exp Anim. 2020; 69: 18–25. [Medline] [CrossRef]
12. Harding JD. Nonhuman Primates and Translational Research: Progress, Opportunities, and Challenges. ILAR J. 2017; 58: 141–150. [Medline] [CrossRef]
13. Konno H, Ishizaka T, Chiba K, Mori K. Ultrasonographic measurement of the renal resistive index in the cynomolgus monkey (Macaca fascicularis) under conscious and ketamine-immobilized conditions. Exp Anim. 2020; 69: 119–126. [Medline] [CrossRef]
14. Lang RM, Badano LP, Mor-Avi V, Afilalo J, Armstrong A, Ernande L, et al. Recommendations for cardiac chamber quantification by echocardiography in adults: an update from the American Society of Echocardiography and the European Association of Cardiovascular Imaging. J Am Soc Echocardiogr. 2015; 28: 1–39.e14. [Medline] [CrossRef]
15. Nakayama S, Koie H, Pai C, Ito-Fujishiro Y, Kanayama K, Sankai T, et al. Echocardiographic evaluation of cardiac function in cynomolgus monkeys over a wide age range. Exp Anim. 2020; 69: 336–344. [Medline] [CrossRef]
16. Ye L, Su L, Wang C, Loo S, Tee G, Tan S, et al. Truncations of the titin Z-disc predispose to a heart failure with preserved ejection phenotype in the context of pressure overload. PLoS One. 2018; 13: e0201498. [Medline] [CrossRef]
17. Ye L, Zhang P, Duval S, Su L, Xiong Q, Zhang J. Thymosin β4 increases the potency of transplanted mesenchymal stem cells for myocardial repair. Circulation. 2013; 128:(Suppl 1): S32–S41. [Medline] [CrossRef]
18. Ye L, D'Agostino G, Loo SJ, Wang CX, Su LP, Tan SH, et al. Early Regenerative Capacity in the Porcine Heart. Circulation. 2018; 138: 2798–2808. [Medline] [CrossRef]
19. Su L, Kong X, Lim S, Loo S, Tan S, Poh K, et al. The prostaglandin H2 analog U-46619 improves the differentiation efficiency of human induced pluripotent stem cells into endothelial cells by activating both p38MAPK and ERK1/2 signaling pathways. Stem Cell Res Ther. 2018; 9: 313. [Medline] [CrossRef]
20. Coelho-Filho OR, Shah RV, Mitchell R, Neilan TG, Moreno H Jr, Simonson B, et al. Quantification of cardiomyocyte hypertrophy by cardiac magnetic resonance: implications for early cardiac remodeling. Circulation. 2013; 128: 1225–1233. [Medline] [CrossRef]
21. Conrad CH, Brooks WW, Hayes JA, Sen S, Robinson KG, Bing OH. Myocardial fibrosis and stiffness with hypertrophy and heart failure in the spontaneously hypertensive rat. Circulation. 1995; 91: 161–170. [Medline] [CrossRef]
22. Nagueh SF, Smiseth OA, Appleton CP, Byrd BF 3rd, Dokainish H, Edvardsen T, et al. Recommendations for the Evaluation of Left Ventricular Diastolic Function by Echocardiography: An Update from the American Society of Echocardiography and the European Association of Cardiovascular Imaging. J Am Soc Echocardiogr. 2016; 29: 277–314. [Medline] [CrossRef]
23. Nagueh SF, Smiseth OA, Appleton CP, Byrd BF 3rd, Dokainish H, Edvardsen T, et al. Houston, Texas; Oslo, Norway; Phoenix, Arizona; Nashville, Tennessee; Hamilton, Ontario, Canada; Uppsala, Sweden; Ghent and Liège, Belgium; Cleveland, Ohio; Novara, Italy; Rochester, Minnesota; Bucharest, Romania; and St. Louis, Missouri. Recommendations for the Evaluation of Left Ventricular Diastolic Function by Echocardiography: An Update from the American Society of Echocardiography and the European Association of Cardiovascular Imaging. Eur Heart J Cardiovasc Imaging. 2016; 17: 1321–1360. [Medline] [CrossRef]
24. Kossaify A, Nasr M. Diastolic dysfunction and the new recommendations for echocardiographic assessment of left ventricular diastolic function: summary of guidelines and novelties in diagnosis and grading. J Diagn Med Sonogr. 2019; 35: 317–325. [CrossRef]